GOSPODARKA SUROWCAMI MINERALNYMI – MINERAL RESOURCES MANAGEMENT

2018 Volume 34 Issue 3 Pages 23–36

DOI: 10.24425/122579

ZEYNEL BASIBUYUK[1], ENGIN EKDUR[2]

Determination of iron minerals with landsat ETM+, Kırşehir, Turkey

Introduction

Study area is located in the Central Anatolia, Turkey which is 30 km long and 16 km wide. The latitudinal and longitudinal extent of the study area is 39°25′42.89″N to 39°15’54.16″N and 33°19′29.38″E to 33°44′13.79″E, respectively. Iron-rich or gossan zones are located in the Upper Cretaceous-aged Central Anatolian Ophiolites and Central Anatolian Granitoids in the region. An iron mine quarry is already being operated in the western part of the study area. This iron-rich and gossan region was used as a reference area in this study. Image processing techniques have been used as the cheapest and fastest method for the interpretation of exploration purposes of large areas. Image processing techniques (band rationing, color composite, PCA) have been commonly used by many researchers to identify iron zones (Tangestani and Moore 2000; Aydal et al. 2007; Madani 2009; Alasta 2011; Ciampalini et al. 2013; Feizi and Mansouri 2013). Iron and gossan content maps were designed using image processing techniques in this study. It is not completely possible to detect operable iron mine deposits through remote sensing methods. The confirmation of iron-rich regions in the maps through field observations indicates that this method can be used as an efficient tool to detect unexplored iron mine deposits in large areas.

✉ Corresponding Author: Engin Ekdur; e-mail: enginekdur@gmail.com

[1] Ahi Evran University, Engineering and Architecture Faculty, Geology Engineering Department, Kırşehir, Turkey; e-mail: zeynelbasibuyuk@gmail.com

[2] Ahi Evran University, Kaman Vocational High School, Map and Cadastre Program, Kırşehir, Turkey; e-mail: enginekdur@gmail.com

1. Geological setting

Units have different ages, geotectonic location and rock types in the Central Anatolian region covering the study area. The exposed formations, in the order of the oldest to the youngest, are as follows: Central Anatolian Metamorphics (Palezoic), Central Anatolian Ophiolits (Upper Cretaceous), Central Anatolian Granitoids (Upper Cretaceous) and cover units (Paleogene–Neogene) (Fig. 1). Central Anatolian Metamorphics are formed by: marble bands, schist, gneiss, quartzite and the amphibolite (Seymen 1981). This formation is tectonically overlain by Central Anatolian Ophiolits which are formed by: gabbro, diabase dikes, basalt, radiolarian, chert, limestone bands, volcanic sandstones and siltstones from bottom to top respectively (Seymen 1981, 1982). In this region, ophiolites emerged in association with an ensimatic island arc on subduction zone (Göncüoğlu and Türeli 1993). Central Anatolian Granitoids are formed by quartz syenite, syenite, alkali feldspar syenite, monzonite, quartz monzonite and granite. They have porphyritic texture along with the presence of pinky-gray and K-feldspar megacrystals on the land and hand-sample level: K-feldspar, plagioclase, quartz, amphibole and biotite mafic minerals include ellipsoid enclaves in up to a 30 cm diameter (Otlu 1998; Boztuğ et al. 2009; Ekincioğlu et al. 2014). Cover units are overlain by all of these units which are formed by sandstone, siltstone, conglomerate, limestone, tuff and gypsum (Kara and Dönmez 1990).

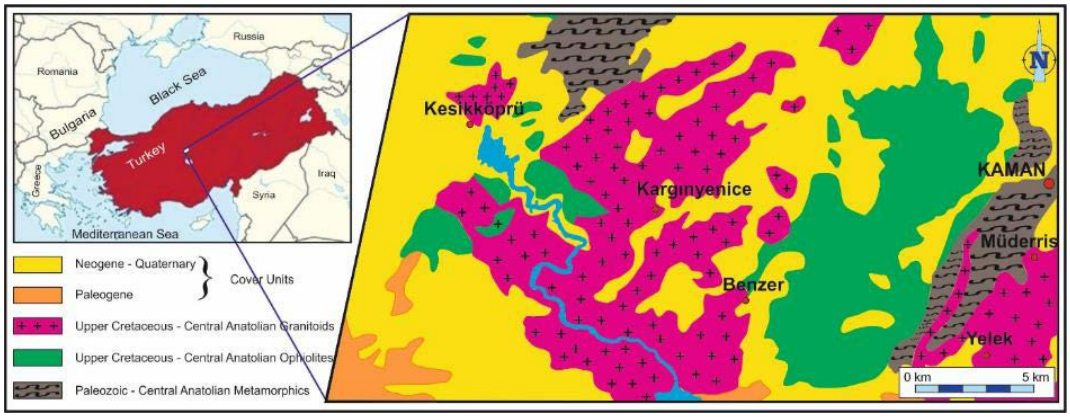

Fig. 1. Geological map of the study area (Kara and Dönmez 1990)

Rys. 1. Mapa geologiczna badanego obszaru

2. Methodologies

The methodology accepted for mapping iron-rich and gossan zones mapping involves two major components namely:

1. Remote sensing based approach
2. Field studies.

Figure 2 shows the adopted methodology. Individual components of the flowchart are described in details as follows. Color composites, band rationing and color composites, PCA analysis and color composites and classification were the image processing techniques used to explore the iron-rich and gossan zones using image data. Iron-rich or gossan zones presented in the obtained satisfactory images were verified with field observations. Images obtained by image processing techniques and field observations were compared and the best methods which identified the enrichment of iron were used in this study.

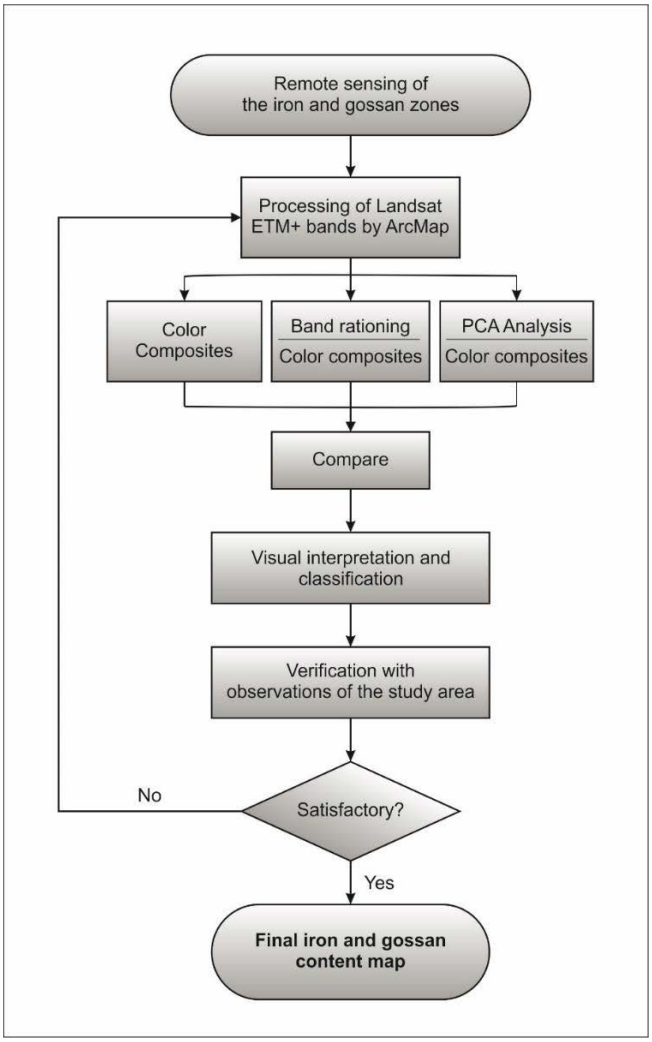

Fig. 2. Flowchart of the methods and technics used

Rys. 2. Schemat wykorzystywanych metod i technik

A subset of Landsat ETM+ (Table 1) scene has been used to evaluate the best approaches for the enhancement of multispectral images to detect iron and gossans zones. The Landsat ETM+ 176/33 image has been used for Kırşehir region, the Central Anatolian. The image was downloaded from the United State Geological Survey website (usgs.gov) and processed via ArcMap 10.2.

Table 1. ETM+ band wavelengths, resolution and technical specifications (nasa.gov)

Tabela 1. Zakresy fal ETM+, rozdzielczość i specyfikacje techniczne

Band Number	µm	Resolution
1	0.45–0.515	30 m
2	0.525–0.605	30 m
3	0.63–0.69	30 m
4	0.775–0.900	30 m
5	1.55–1.75	30 m
6	10.4–12.5	60 m
7	2.08–2.35	30 m
8	0.52–0.90	15 m
ETM+ technical specifications		
Sensor type: opto-mechanical Spatial Resolution: 30 m (60 m – thermal, 15 m pan) Spectral Range: 0.45–12.5 µm Number of Bands: 8 Temporal Resolution: 16 days Image Size: 183 × 170 km Swath: 183 km Programmable: yes		

Bands 1, 2, 3, 4, 5 and 7 of Landsat ETM+ images were usually used to determine lithology, mineral abundance and natural sources (Kaufmann 1988; Sabins 1999; Gupta 2003; Dogan 2008; Madani 2009; Alasta 2011; Ciampalini et al. 2013). Crippen (1989) proved tripling combination technique using correlation coefficient of images. Drury (2001) chose 3 band (742 as RGB) which can give geological information. However, the iron-rich and gossan zones could not be visually distinguished on this image.

Iron oxide, clay minerals and sulphate minerals associated with hydrothermally altered or weathered rocks have been investigated using band ratios (Kaufmann 1988; Sabins 1999; Madani 2009; Ciampalini et al. 2013). Iron minerals highly absorb electromagnetic waves

for Landsat 7 ETM+ band 1 and highly reflect for bands 3, 4, 5 and 7 (Fig. 3). According to Sabins (1999), Ciampalini et al. (2013) and Kaufman (1988), iron-rich and gossan zones are highlighted on the obtained images which use the ratio of band 3 to band 1 (3/1), ratio of band 4 to band 1 (4/1) and the ratio of bands 5 and 7 to band 1 (5/1–7/1), respectively.

Both band rationing and band composite techniques are used to detect lithology, mineral abundance and natural resources by some researchers. As suggested by Abrams et al. (1983), Sabins (1999), Elsayed and Albiely (2008), Ciampalini et al. (2013) used the combination of the ratios 5/7:3/2:4/3, 3/5:3/1:5/7, 5/7:5/4:3/1 and 5/7:3/1:4/3, 3/5:4/1:5/7, respectively in order to detect altered rocks characterized by both ferric iron and hydrothermal clays.

The PCA (Principal Component Analysis) is a multivariate statistical technique that selects uncorrelated linear combinations (eigenvector loadings) of variables in such a way that each successively extracted linear combination or principal component (PC) has a smaller variance (Singh-Harrison 1985). The PCA is widely used to compress the multispectral data sets by calculating a new coordinate system. PCA is usually used for mapping lithologies, minerals and alterations (Abrams et al. 1997; Kaufman 1988; Loughlin, 1991; Tangestani and Moore, 2001). The standard PCA (bands 1, 2, 3, 4, 5 and 7) and Developed Selected PCA (Crosta Technique) were used in this study. A Crosta Technique using sets of four selected image bands is developed to depict hydroxyl (bands 1, 4, 5 and 7) and iron-oxide (bands 1, 3, 4 and 5), alteration zones (Crosta and Moore 1989; Loughlin 1991; Rutz-Armenta and Prol-Ledesma 1998; Ciampalini et al. 2013; Tangestani-Moore 2000, 2001).

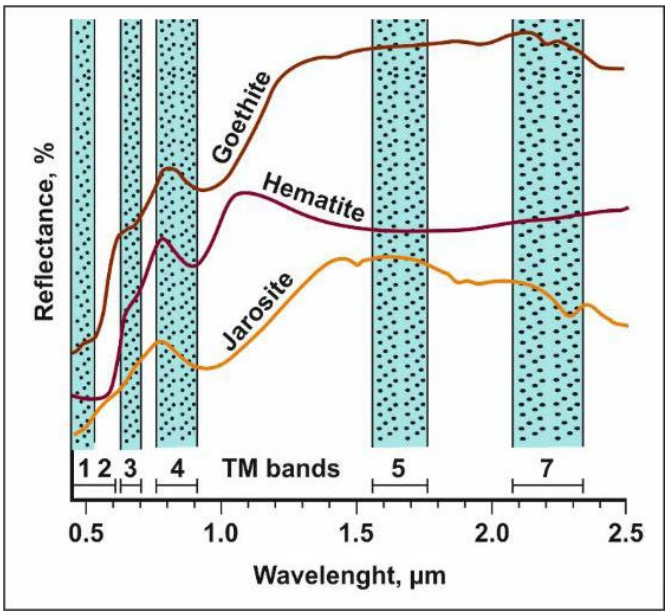

Fig. 3. Spectral library plots from NASA library for iron oxide minerals

Rys. 3. Biblioteka spektralna dla minerałów tlenku żelaza z biblioteki NASA

According to Ciampalini et al. (2013), iron-rich and gossan zones may be determined using PCs bands combinations as well and the best combination is represented by PCs 4, 3 and 2 as RGB.

3. Results and discussions

Four iron-rich and gossan zones have been identified at the end of the image processing techniques and field observations. These zones are presented in ellipses on the obtained images. The obtained results are given below.

3.1. Band ratios

The band ratios of Landsat ETM+ have been extensively used to produce geological, mineral abundance and alteration maps. According to Sabins (1999) and Ciampalini et al. (2013), iron-rich and gossan zones are highlighted on the obtained images which use the ratio of bands 3 and 4 to band 1 (3/1–4/1). At the same time, Kaufman (1988) reported to have identified iron-rich and gossan zones using ratio of bands 5 and 7 to band 1 (5/1–7/1). The best result was obtained by 4/1 band ratio in this study. Iron-rich or gossan zones have been brightly presented on invert of 4/1 ratio image. However, iron-rich and gossan zones are still not clearly distinguished (Fig. 4).

Iron rich and gossan zones have been transformed into reddish color by unsupervised classification applied to 4/1 image. Although this image does not contain iron, reddish regions are seen. Therefore, this method is not useful for the detection of iron-rich and gossan zones in this area.

As suggested by Abrams et al. (1983), Sabins (1999), Essayed and Albiely (2008), Ciampalini et al. (2013) used the combination of the ratios 5/7:3/2:4/3, 3/5:3/1:5/7, 5/7:5/4:3/1 and 5/7:3/1:4/3, 3/5:4/1:5/7, respectively, to detect altered rocks characterized by both ferric iron and hydrothermal clays. All of these methods have been applied and the best result was obtained from 3/5:4/1:5/7 image (Fig. 6). Other color composite was proved to be notably useful for highlighting the areas characterized by the presence of iron ore deposits in the study area. Iron rich and gossan zones have been transformed into reddish color by unsupervised classification applied to the 3/5:4/1:5/7 image (Fig. 7). The image was obtained through this method which is found successful for the detection of iron-rich and gossan zones.

3.2. Principle Component Analyses (PCA)

Correlation matrix values and eigenvector loadings of the Landsat 7 ETM+ bands (1, 2, 3, 4, 5 and 7 – Standard PCA) used in this study are presented in Table 2 and 3. There was

a difference between the highest eigenvector loading for band 1 (0.83) and band 4 (–0.38) in the PC3 band. Iron-rich or gossan zones have been brightly presented on the PC3 image (Fig. 8). Iron rich zones have been transformed into reddish color by unsupervised classification applied to the PC3 image (Fig. 9). The image was obtained through this method which is found successful for the detection of iron-rich and gossan zones. Images obtained by this image processing technique indicate the iron density map for study area. Iron density is increasing from yellow to red.

Table 2. Correlation matrix of the study area

Tabela 2. Macierz korelacji na badanym obszarze

ETM+ Bands	Band 1	Band 2	Band 3	Band 4	Band 5	Band 7
Band 1	1.00	0.98	0.91	0.86	0.95	0.91
Band 2	0.98	1.00	0.97	0.82	1.00	0.98
Band 3	0.91	0.97	1.00	0.69	0.98	1.00
Band 4	0.86	0.82	0.69	1.00	0.80	0.70
Band 5	0.95	1.00	0.98	0.80	1.00	0.98
Band 7	0.91	0.98	1.00	0.70	0.98	1.00

Table 3. Eigenvector loadings for the study area

Tabela 3. Obciążenia własne dla obszaru badania

	PC1	PC2	PC3	PC4	PC5	PC6
Band 1	0.34	0.28	0.83	0.06	0.24	–0.22
Band 2	0.32	0.05	0.21	–0.25	–0.54	0.70
Band 3	0.40	–0.33	–0.13	0.37	0.60	0.47
Band 4	0.26	0.82	–0.38	0.33	–0.04	0.04
Band 5	0.58	–0.02	–0.30	–0.68	0.18	–0.27
Band 7	0.47	–0.37	–0.06	0.47	–0.51	–0.40
Eigenvalue variance (%)	94.38	4.69	0.65	0.18	0.09	0.01

The correlation matrix values and eigenvector loadings of the Landsat 7 ETM+ bands (1, 3, 4, 5 – Developed Selected the PCA – Crosta Technique) used in this study presented in Table 4 and Table 5. There was a difference between the highest eigenvector loading for band

Table 4. Correlation matrix for iron oxides mapping of the study area

Tabela 4. Macierz korelacji dla mapowania tlenków żelaza w badanym obszarze

ETM+ Bands	Band 1	Band 3	Band 4	Band 5
Band 1	1.00	0.91	0.86	0.95
Band 3	0.91	1.00	0.69	0.98
Band 4	0.86	0.69	1.00	0.80
Band 5	0.95	0.98	0.80	1.00

Table 5. Eigenvector loadings for iron oxides mapping of the study area

Tabela 5. Obciążenia własne dla mapowania tlenków żelaza w badanym obszarze

ETM+ Bands	Band 1	Band 3	Band 4	Band 5
Band 1	0.42	0.21	0.88	–0.05
Band 3	0.48	–0.46	–0.08	0.74
Band 4	0.32	0.84	–0.33	0.28
Band 5	0.70	–0.20	–0.32	–0.61
Eigenvalue variance (%)	93.22	5.72	0.95	0.11

1 (0.88) and band 4 (–0,33) in the PC4 band. Iron-rich or gossan zones have been brightly presented on PC4 image (Fig. 10). Iron rich and gossan zones have been transformed into reddish color by unsupervised classification applied to the PC4 image (Fig. 11). The image was obtained through this method which is found successful for the detection of iron-rich and gossan zones. Images obtained by this image processing technique indicate the iron

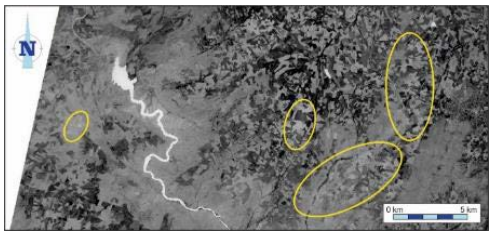

Fig. 4. Invert of the ratio image of ETM+ bands 4/1 in study area

Rys. 4. Odwrócenie proporcji obrazu ETM + pasm 4/1 w obszarze badania

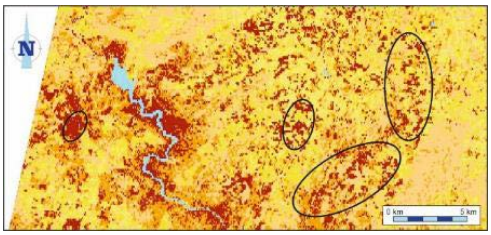

Fig. 5. Unsupervised Classification (6 Class) of ETM+ band ratios 4/1

Rys. 5. Klasyfikacja bez nadzoru (klasa 6) proporcji pasma ETM + 4/1

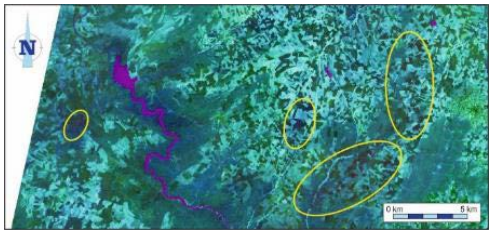

Fig. 6. ETM+ band ratios 3/5, 4/1 and 5/7 as RGB, respectively. The presence of iron oxides corresponds to the violet zones in the ellipses

Rys. 6. Proporcje pasma ETM + odpowiednio 3/5, 4/1 i 5/7 jako RGB. Obecność tlenków żelaza odpowiada strefom fioletowym w elipsach

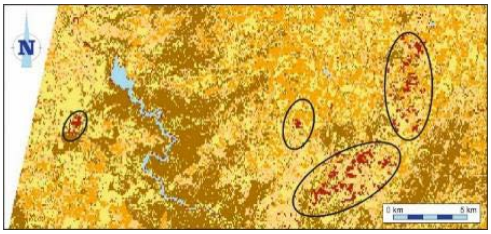

Fig. 7. Unsupervised Classification (6 Class) of ETM+ band ratios 3/5, 4/1 and 5/7 as RGB, respectively. The presence of iron oxides corresponds to the reddish zones in the ellipses

Rys. 7. Klasyfikacja bez nadzoru (klasa 6) proporcji pasma ETM + odpowiednio 3/5, 4/1 i 5/7 jako RGB. Obecność tlenków żelaza odpowiada czerwonawym strefom w elipsach

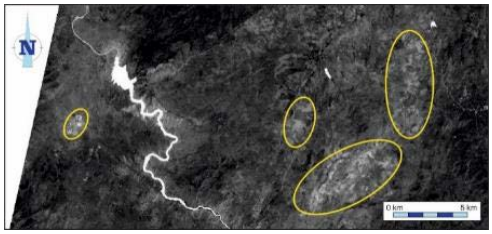

Fig. 8. PC3 image of standardized transformation. The presence of iron oxides corresponds to the brightest zone

Rys. 8. Obraz PC3 transformacji standaryzowanej. Obecność tlenków żelaza odpowiada najjaśniejszej strefie

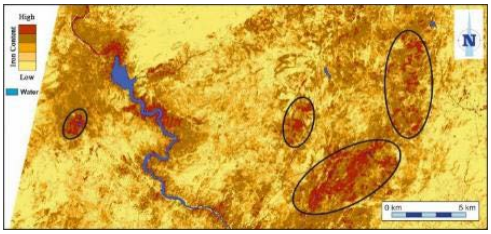

Fig. 9. Unsupervised Classification of PC3. The presence of iron oxides corresponds to the reddish zones in the ellipses

Rys. 9. Klasyfikacja PC3 bez nadzoru. Obecność tlenków żelaza odpowiada czerwonawym strefom w elipsach

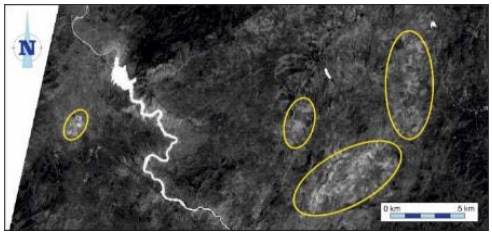

Fig. 10. PC4 image obtained using the Crosta Technique. The presence of iron oxides corresponds to the brightest zone

Rys. 10. Obraz PC4 uzyskany za pomocą Crosta Technique. Obecność tlenków żelaza odpowiada najjaśniejszej strefie

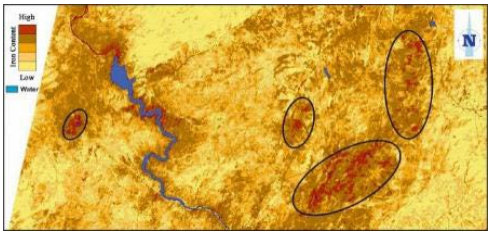

Fig. 11. Unsupervised Classification of PC4. The presence of iron oxides corresponds to the reddish zones in the ellipses

Rys. 11. Klasyfikacja PC4 bez nadzoru. Obecność tlenków żelaza odpowiada czerwonawym strefom w elipsach

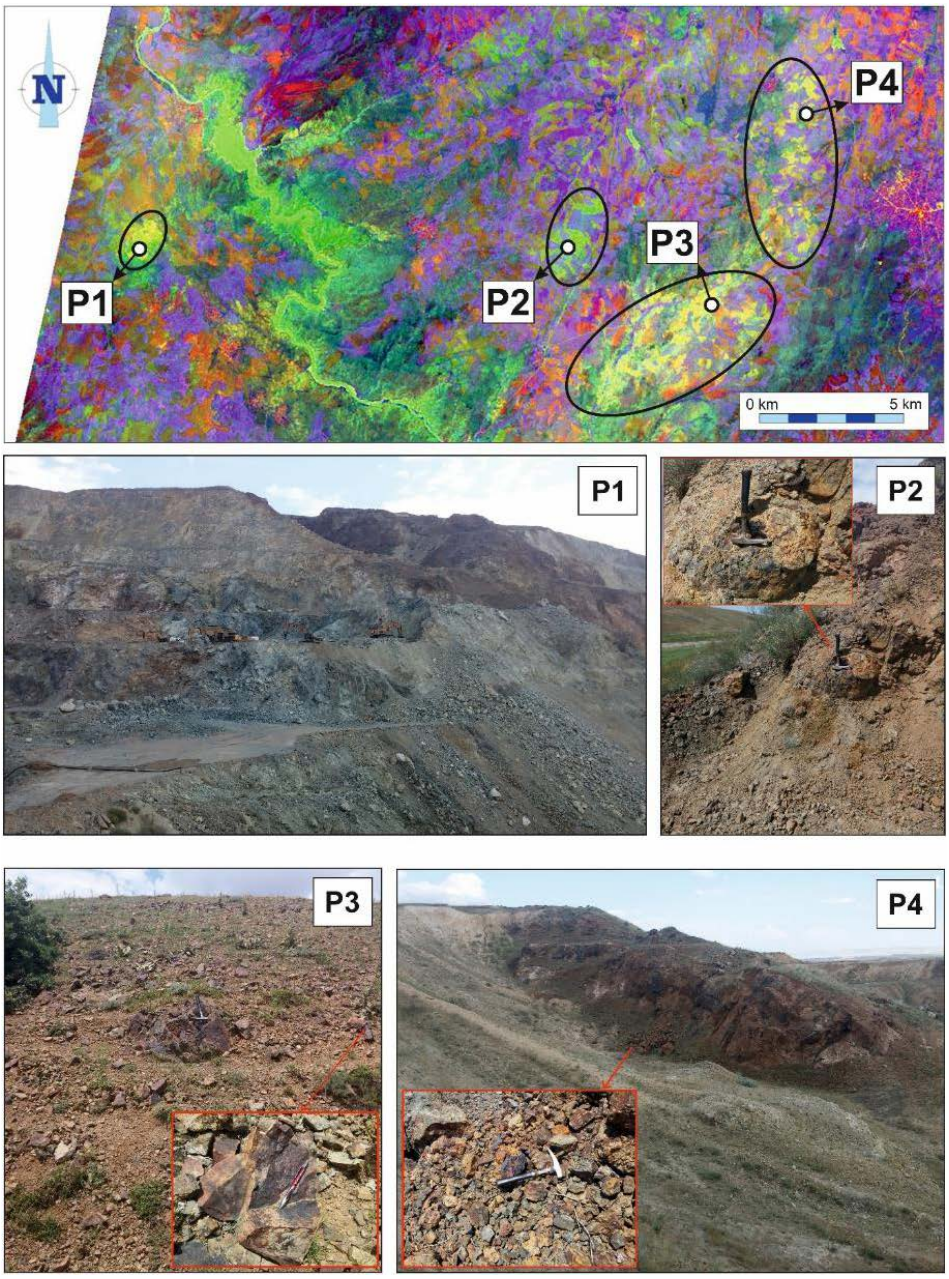

Fig. 12. ETM+ band combination of PC4, PC3 and PC2 as RGB.
The presence of iron oxides corresponds to the yellowish green zones in the ellipses. P1, P2, P3 and P4 are marked each location of the taken photos which iron-rich and gossan zones

Rys. 12. ETM + kombinacja pasm odpowiednio PC4, PC3 i PC2 jako RGB.
Obecność tlenków żelaza odpowiada żółtawo-zielonym strefom w elipsach. P1, P2, P3 i P4 oznaczają każdą lokalizacją zrobionych zdjęć, które zawierają strefy bogate w żelazo i strefy gossan

density map for study area. Iron density is increasing from yellow to red. This method gives similar results considering the iron concentration in the Standard PCA. However, reddish zones being among most intense zones which are decreasing in Crosta Technique.

Iron rich and gossan zones have been transformed into yellowish green color on the PC4:PC3:PC2 color composite image (Fig. 12). The image was obtained through this method which is found successful for the detection of iron-rich and gossan zones.

In images obtained through the 4/1, 3/5:4/1:5/7, PCA (PC3) and Crosta (1, 3, 4 and 5 bands) methods, iron-rich regions and water areas cannot be distinguished from each other. However, these areas have been through unsupervised classification via these images.

These zones, 3 are located in the Central Anatolia Ophiolites and 1 is located in the Central Anatolia Granitoids.

The P1 location takes place in the Central Anatolia Ophiolites as presented in Figure 12 is the iron mining area which has belonged to Özce Mining since 1983 and extracts 100,000 tons per year. In this land, iron-rich zones are observed as iron veins reaching up to 50 m. This location was used as a reference area for the application of remote sensing techniques used to determine the iron-rich and gossan zones and satisfying photos. The gossan zone in the P3 locations taking place in Central Anatolia Ophiolites involve iron plaster with several mm thickness, on the other hand, the gossan zone in the P4 location involve several cm of low iron content lenses and veins. The gossan zone in Central Anatolia Granitoids are within the alteration levels and involves several cm of low iron content lenses and veins (P2 – Fig. 12).

Band rationing, PCA analysis, unsupervised classification, band rationing and color composites and PCA analysis and color composites were image processing techniques used to explore the iron-rich and gossan zones using image data. All of these methods can be used for exploring the iron-rich and gossan zones.

Despite the presence of iron deposits in these areas, all these areas are not in operable quality. It was observed that iron rich and gossan zones could be detected through remote sensing techniques to a great extent. This study shows that remote sensing techniques offer significant advantages to detect iron rich and gossan zones; yet it is compulsory to confirm detected operable iron mines through field observations.

REFERENCES

Abrams et al. 1983 – Abrams, M.J., Brown, D., Lepley, L. and Sadowski, R. 1983. Remote sensing for porphyry copper deposits in Southern Arizona. *Economic Geology* 78, pp. 59–604.

Abrams et al. 1997 – Abrams, M., Kishino, M. and Matsunaga, T. 1997. Future uses of EOS ASTER data for hydrologic applications, ERIM 4th International Conference on Remote Sensing for Marine and Coastal Applications, held in Orlando, Florida.

Alasta, A.F. 2011. Using remote sensing data to indentify iron composite in central western Libya, International conference on Emerging trends in Computer and Image processing, Bangkok, pp. 56–61.

Aydal et al. 2007 – Aydal, D., Vural, A., Uslu (Taşdelen), I. and ve Aydal, E.G. 2007. Investigation of Alakeçi-Kisacik (Bayramiç-Balıkesir) Mineralization Zone with Crosta Technique Using Landsat 7 ETM+. *Journal of the*

Faculty of Architecture and Engineering, Selcuk University Vol. 23, Issue 3, pp. 29–40.

Boztug et al. 2009 – Boztug, D., Güney, Ö., Heizler, M., Jonckheere, R.C., Tichomirowa, M. and Otlu, N. 2009. 207Pb-206Pb, 40Ar-39Ar and fission-track geothermochronology quantifying cooling and exhumation history of the Kaman-Kırsehir region intrusions, Central Anatolia, Turkey. *Turkish Journal of Earth Sciences* 18(1), pp. 85–108.

Ciampalini, et al. 2013 – Ciampalini, A., Garfagnoli, F., Antonielli, B., Moretti, S. and Righini, G. 2013. Remote sensing techniques using Landsat ETM+ applied to the detection of iron ore deposits in Western Africa. *Arab J Geoscience* 6, pp. 4529–4546

Crippen, R.E. 1989. Selection of Landsat TM band and band-ratio combinations to maximize lithologic information in color composite displays In: Proceedings of the 7th Thematic Conference on remote sensing for exploration geology, Vol. II, *Environmental Research Institute of Michigan, Ann Arbor, Mich.*, pp. 917–921.

Crosta, A. and Moore, J. McM. 1989. *Enhancement of Landsat Thematic Mapper imagery for residual soil mapping in SW Minais Gerais State, Brazil: a prospecting case history in Greenstone belt terrain* [In:] *Proceedings of the 7th ERIM Thematic Conference: Remote sensing for exploration geology*, pp. 1173–1187.

Dogan H.M. 2008. Applications of Remote Sensing and Geographic Information Systems to Assess Ferrous Minerals and Iron Oxide of Tokat Province in Turkey. *International Journal of Remote Sensing* 29(1), pp. 221–233.

Drury, S.A. 2001. *Image Interpretation in Geology*, 3. edn. Allen & Unwin, London

Ekincioğlu et al. 2014 – Ekincioğlu, G., Başıbüyük, Z., Ekdur, E., Ballı, F. and Kanbir, E.S. 2014. *Kırşehir Natural Stone Sector Analysis and Report of Investment Opportunities*, 116 p.

Elsayed K.A. and Albiely A.I. 2008. Ratio image processing techniques: a prospecting tool for mineral deposits, Red Sea Hills, NE Sudan. *Int Arch Photogramm Remote Sens Spat Inf Sci* 37, pp. 1295–1298

Feizi, F. and Mansouri, E. (2013. Introducing the Iron Potential Zones Using Remote Sensing Studies in South of Qom Province, Iran. *Open Journal of Geology* 3, pp. 278–286.

Göncüoglu, M.C. and Türeli, K. 1993. Petrology and geodynamic interpretation of plagiogranites from Central Anatolian ophiolites (Aksaray–Turkey), Turkish Journal of Earth Sciences.

Gupta, Ravi P. 2003. Remote Sensing Geology, second ed. Springer, Berlin, New York. 655 p.

Kara, H. and Dönmez, M. 1990. 1/100,000 scale Geological Map of Turkey series. Kırşehir-G-17 Sheet MTA Publications Turkey Geological Map Series of the G-17 Sheet.

Kaufman, H. 1988. Mineral exploration along the Agaba–Levant structure by use of TM-data concepts, processing and results. *International Journal of Remote Sensing* 9, pp. 1639–1658.

Loughlin, W.P. 1991. Principal component analysis for alteration mapping. *J Photogramm Eng Rem Sens* 57, pp. 1163–1169.

Madani, A.A. 2009. Utilization of Landsat ETM+ Data for Mapping Gossans and Iron Rich Zones Exposed at Bahrah Area, Western Arabian Shield, Saudi Arabia. Earth Science, 20 (1) 35-49.

Otlu, N. 1998. Petrological Investigation of Plutonic Rocks Between Kortundağ-Baranadağ (D Kaman, Kırşehir). Cumhuriyet University, Institute of Science and Technology, Doctorate Thesis 1998. 164 p.

Rutz-Armenta, J. R. and Prol-Ledesma, R. M. 1998. Techniques for enhancing the spectral response of hydrothermal alteration minerals in Thematic Mapper images of Central Mexico. *International Journal of Remote Sensing* 19, pp. 1981–2000.

Sabins, F.F. 1999. Remote sensing for mineral exploration. *Ore Geol. Rev* 14, pp. 157–183

Seymen, I. 1981. Stratigraphy and metamorphism of the Kırşehir Massif around Kaman (Kırşehir). *Geological Bulletin of Turkey* 24/2, pp. 7–14.

Singh, A. and Harrison A. 1985. Standardized principal components. *International Journal of Remote Sensing* 6, pp. 883–896.

Tangestani, M.H. and ve Moore, F. 2000. Iron oxide and hydroxyl enhancement using the Crosta Method: a case study from the Zagros Belt, Fars province, Iran. *Communication, JAG* 2, pp. 140–146.

Tangestani, M.H. and ve Moore, F. 2001. Comparison of three principal component analysis techniques to porphyry copper alteration mapping. A case study, Meiduk area, Kerman, Iran. *Canadian Journal of Remote Sensing* 27, pp. 176–182.

DETERMINATION OF IRON MINERALS WITH LANDSAT ETM+, KIRŞEHIR, TURKEY

Abstract

Image processing techniques (band rationing, color composite, Principal Component Analyses) are widely used by many researchers to describe various mines and minerals. The primary aim of this study is to use remote sensing data to identify iron deposits and gossans located in Kaman, Kırşehir region in the central part of Anatolia, Turkey. Capability of image processing techniques is proved to be highly useful to detect iron and gossan zones. Landsat ETM+ was used to create remote sensing images with the purpose of enhancing iron and gossan detection by applying ArcMap image processing techniques. The methods used for mapping iron and gossan area are 3/1 band rationing, 3/5 : 1/3 : 5/7 color composite, third PC and PC4 : PC3 : PC2 as RGB which obtained result from Standard Principal Component Analysis and third PC which obtained result from Developed Selected Principal Component Analyses (Crosta Technique), respectively. Iron-rich or gossan zones were mapped through classification technique applied to obtained images. Iron and gossan content maps were designed as final products. These data were confirmed by field observations. It was observed that iron rich and gossan zones could be detected through remote sensing techniques to a great extent. This study shows that remote sensing techniques offer significant advantages to detect iron rich and gossan zones. It is necessary to confirm the iron deposites and gossan zones that have been detected for the time being through field observations.

Keywords: remote sensing, image processing, mineral mapping, hematite, goethite

WYKORZYSTANIE DANYCH TELEDETEKCYJNYCH DO IDENTYFIKACJI ZŁÓŻ ŻELAZA Z LANDSAT ETM+, KIRŞEHIR, TURCJA

Streszczenie

Głównym celem tego artykułu jest wykorzystanie danych teledetekcyjnych do identyfikacji złóż żelaza i gossan (rdzawe tlenkowe i wodorotlenkowe minerały żelaza i manganu, które występują nad złożem rudy) znajdujących się w Kaman, w regionie Kırşehir, w centralnej części Anatolii, w Turcji. Udowodniono, że możliwości przetwarzania obrazów są bardzo użyteczne w wykrywaniu stref żelaza i gossan. Landsat ETM+ został użyty do stworzenia obrazów teledetekcyjnych w celu poprawy wykrywania złóż żelaza i gossan poprzez zastosowanie ArcMap technik przetwarzania obrazu. Metody mapowania złóż żelaza i gossan stosują proporcje pasma 3/1, złożoność koloru 3/5: 1/3: 5/7, trzeci główny składnik PC (*Principal Component*) uzyskany w wyniku Developed Selected PCA (*Crosta Technique*) i proporcje PC4: PC3: PC2 jako RGB uzyskane w wyniku standardowej analizy głównych składowych PCA (*Principal Component Analysis*). Strefy bogate w żelazo lub strefy gossan zostały odwzorowane za pomocą techniki klasyfikacji zastosowanej do uzyskanych obrazów. Mapy zawartości żelaza i gossan zaprojektowano jako produkty końcowe. Dane te zostały potwierdzone w obserwacjach terenowych. Zaobserwowano, że strefy bogate w żelazo i strefy gossan mogą być w dużym stopniu wykrywane za pomocą technik teledetekcji.

Badanie to pokazuje, że techniki teledetekcji dają znaczne korzyści w wykrywaniu stref bogatych w żelazo i gossan; jednak koniecznie należy potwierdzić wykryte złoża żelaza za pomocą obserwacji terenowych.

Słowa kluczowe: teledetekcja, przetwarzanie obrazu, mapowanie mineralne, hematyt, getyt